One-Step Hydrothermal Synthesis of pH-mediated Histidine Carbon Dots for Bio-imaging and White Light Emission

M.Sc. Thesis

By

Saikat Sinha

DISCIPLINE OF CHEMISTRY

INDIAN INSTITUTE OF TECHNOLOGY INDORE

MAY, 2023

One-Step Hydrothermal Synthesis of pH-mediated Histidine Carbon Dots for Bio-imaging and White Light Emission

A THESIS

Submitted in fulfillment of the
requirements for the award of the degree
of
Master of Science

by
Saikat Sinha

DISCIPLINE OF CHEMISTRY
INDIAN INSTITUTE OF TECHNOLOGY INDORE
MAY, 2023

INDIAN INSTITUTE OF TECHNOLOGY INDORE

DECLARATION

I hereby certify that the work which is being presented in the report entitled **One-Step Hydrothermal Synthesis of pH-mediated Histidine Carbon Dots for Bio-imaging and White Light Emission** in fulfillment of the requirements for the award of the degree of **MASTER OF SCIENCE** and submitted in the **DEPARTMENT OF CHEMISTRY**, **Indian Institute of Technology Indore**, is an authentic record of my own work carried out during the period of **July 2022** to **May 2023** under the supervision of **Prof. Anjan Chakraborty**, Professor, IIT Indore.

The matter presented in this thesis has not been submitted by me for the award of any other degree of this or any other institute.

Saikat Sinha 25/05/2023

Signature of the student with date
Saikat Sinha

This is to certify that the above statement made by the candidate is correct to the best of my/our knowledge.

A Chakraborty

25/05/2023

Signature of the Supervisor with date
Prof. Anjan Chakraborty

Saikat Sinha has successfully given his M.Sc. Thesis (Stage II) Examination held on **17th May 2023.**

A Chakraborty

Signature of Supervisor of **M.Sc. Thesis**

Date: 25/05/2023

Convenor, **DPGC**

29/05/2023

Date:

Signature of the **PSPC** Member

Date: 25/05/2023

Signature of **PSPC** Member

Date: 29/5/23

ACKNOWLEDGEMENT

First and foremost, I want to thank my supervisor, **Prof. Anjan Chakraborty** for his guidance and constant supervision during the project work. I thank him not only for providing lab facilities but also for his motivation towards research and advice for the future of my life.

I would also like to thank **Dr. Tridib Kumar Sarma** and **Prof. Tushar Kanti Mukherjee** for their help in various aspects.

I am very much grateful to **Mr. Avijit Maity** for his valuable suggestion and continuous help in every field of this project. He motivates me throughout this project and his suggestions in every aspect of life motivate me to study and understand not only this subject but various other aspects.

I want to thank Mr. Debanjan Bagchi, Ms. Huma Tabassum, Mr. Sachin Debnath, Ms. Priyanka Nath, and Ms. Aditi Maheswari, for their constant support throughout this project.

Moreover, I am filled with gratitude to my family and friends for staying with me in my bad times.

Finally, I truly admire SIC, IIT Indore, and IIT Indore for providing all the facilities to conduct my research project.

Saikat Sinha

MSc 2nd year

Abstract

Carbon Dots have promising applications in optics, catalysis, sensing, etc. Single precursor-based white light-emitting carbon dots are very rare. In the present contribution, we aim to synthesize pH mediated (~8 and <1) histidine carbon dots and their photophysical properties. His-pH1 CD and His-pH8 showed bluish-white emission and blue emission behavior in water medium under UV light. His-pH1 CD showed aggregation-induced white emission in ethanol whereas His-pH8 CD does not. A sharp decrement in intensity was observed for His-pH 1 CD as soon as the pH decreased from 7 to 6. So, it can be used as a pH-based sensor. Furthermore, we have studied the interaction with lipid vesicles which reveals the discriminatory behavior of lipid vesicles towards as synthesized pH-mediated carbon dots. White light was obtained through His-pH1 polymer composites.

TABLE OF CONTENT

LIST OF FIGURES

NOMENCLATURE

CD	Carbon Dot
°C	Degree centigrade
DI	De-ionized
τ_i	Lifetime of the i^{th} component
mbar	millibar
nm	Nanometer
QY	Quantum Yield
χ^2	Reduced chi-Square Amplitude

ACRONYMS

CLSM	Confocal Laser Scanning Microscopy
CND	Carbon nano Dots
CQD	Carbon Quantum Dot
DMPC	1,2-dimyristoyl-sn-glycero-3- Phosphocholine
GQD	Graphene Quantum Dot
TCSPC	Time-Correlated Single Photon Counting

Introduction

1.1 Nanomaterials and Nanoparticles:

For the past few decades, the development of nanomaterials and nanotechnology is one of the central fascinating fields of science. The word nano signifies the dimension which is in nanometers (nm) level ranging from 1-100 nm. The size and shape of nanomaterials depend on various synthetic techniques which govern the physical and optical properties of nanomaterials. One can imagine the dimension of nanoparticles (NPs) by linearly combining 10 hydrogen atoms which is 1 nm. Talking about the history of NPs, the word nanometre was first introduced by Richard Adolf Zsigmondy [1]. The specific concept of nanotechnology was introduced by Sir Richard Feynman in 1959 who is considered the father of nanotechnology. In 1959 he delivered a lecture in which he talked about writing the whole Encyclopaedia Britannica on a tip of a pin [2,3]. The term nanotechnology was first introduced by Norio Taniguchi in 1974 [4,5]. Based on their size and morphology, Nanoparticles can be classified into carbon nanoparticles, metal nanoparticles, inorganic semiconductor nanoparticles, polymeric nanoparticles [6-12]. Talking about morphology, NPs exhibit unique morphologies like nanorods, nanoshells, nanocages, nanoflowers, nanostars, nanofibers [13-16] which are directly connected to synthetic methodologies.

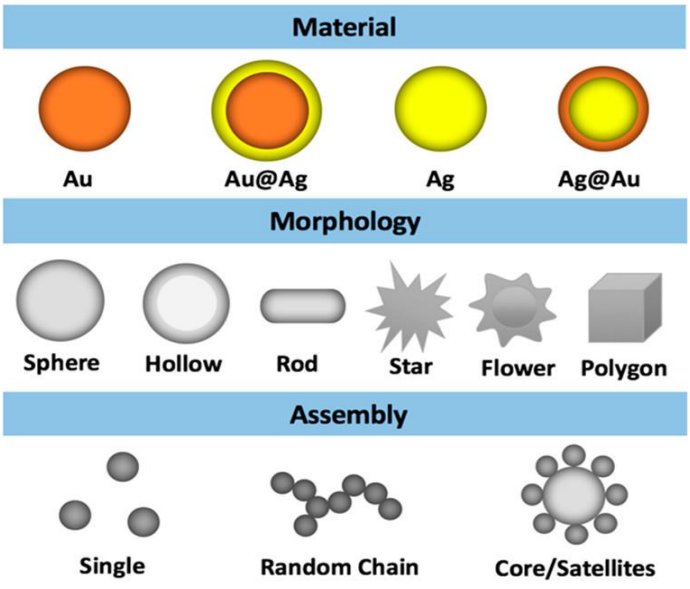

Figure 1: Various morphologies of nanoparticles [17].

1.2 Carbon Dots (CDs): A General Overview:

Carbon dots arrived in the modern era of science due to their luminescent property [18]. It has a diameter of <10 nm and its core consists of a sp^2/sp^3 hybrid carbon framework along with abundant functional groups on its surface [19,20]. The advantages that make carbon dots unique are low toxicity, unique optical properties, tunable emission wavelength, excellent photostability, non-blinking, upconversion emission, excellent biocompatibility, resistance to photobleaching, eco-friendly synthesis, small size, easy functionalization, high quantum yield [21-26]. In 2004, fluorescent carbon nanomaterials were first reported by Xu et al [27] and since then much research has been done on carbon dots (CD), and CDs have garnered enormous attraction among researchers, due to the above factors. Based on the above factors carbon dots have significant applications such as catalysis, optoelectronic devices such as LED, solar cells, bioimaging and drug delivery, sensing, security, and anti-counterfeiting [28-38]. Based on the dimensions CDs can be classified into four categories. In zero-dimensional CDs, like quantum dots, Carbon dots, core-shell quantum dots, onions, and nano lenses; all the dimensions (x, y, z) lie in the manometer range (1-100 nm), which is none of the dimensions are outside the nanoscale range. In the case of one-dimensional such as nanowires, nanorods, nanotubes, nanoribbons; two-dimensional nanomaterials such as nanoplates, nanosheets, and nanodisks; and three-dimensional nanomaterials such as nanoballs (dendritic structures), nano coils, nanocones, and nanoflowers; they are having one, two, and three dimensions outside the nanoscale respectively [39,40].

1.3 Synthesis of Carbon Dots:

There are mainly, two basic approaches followed for synthesizing carbon dots:

1.3.1 The Top-Down approach: In the Top-Down approach involves massive carbon compounds such as graphene oxide sheets, graphene, carbon fibers, and carbon nanotubes sliced or broken down into nanosized particles via several methods such as Arc Discharge Method, Laser Ablation Method, Ultrasonic Method, Chemical Oxidation Method.

1.3.2 The Bottom-Up approach: In this process selected precursor molecules to transform into quantum-sized particles through a variety of methodologies like hydrothermal techniques, microwave techniques, thermal techniques, and template techniques.

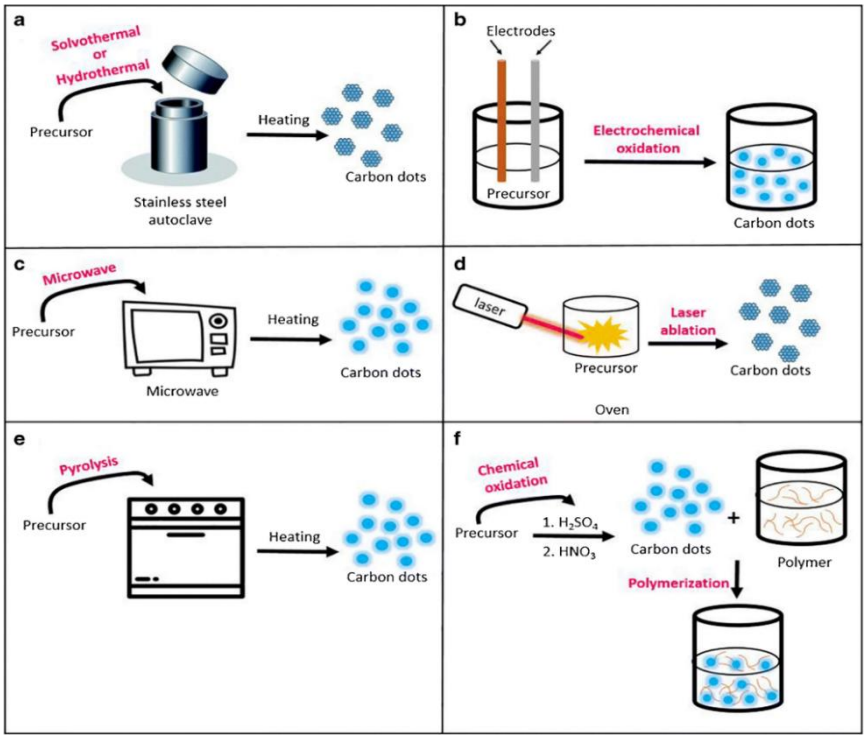

Figure 2: Different synthetic procedures of carbon dots [41].

1.4 Classification of Carbon Dots:

1.4.1 Graphene Quantum Dots (GQD):

These are single-layer or multi-layer flaky crystalline nanoparticles with conjugated π-electron graphene layers that also exhibit the quantum confinement Effect.

1.4.2. Carbon Quantum Dots (CQD):

The CQDs are always spherical and have crystal lattices and different functional groups on their surface, which show intrinsic state luminescence and quantum confinement effect of the carbon quantum dots due to different sizes. So, it is important to regulate the wavelength of photoluminescence through the tuning of the carbon quantum dot's size, which opens new avenues in the field of nanotechnology [42].

1.4.3. Carbon Nanodots (CND):

The CNDs have a high degree of carbonization with different functional groups on the surface. In general, crystal lattice structure and polymer features were absent and the luminescence arises from the defects or surface state and subdomain state within the graphitic carbon core [43].

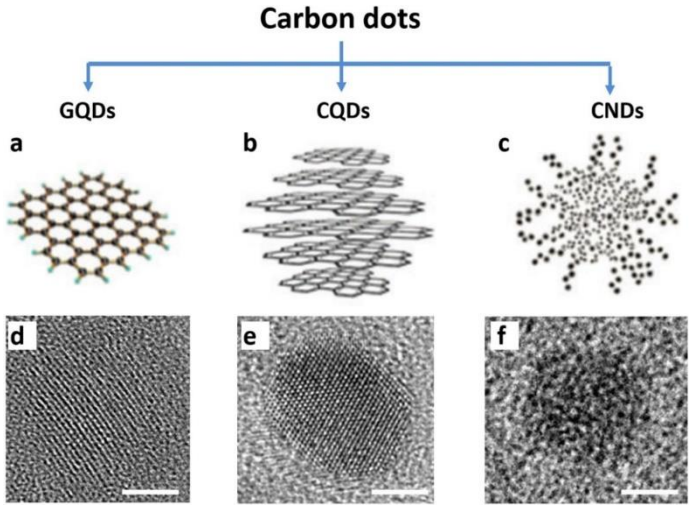

Figure 3: (a) GQD (b) CQD (c) CND structures. HRTEM images of (d) GQD (e) CQD (f) CND [44].

1.5 Interaction of CDs with Lipid Vesicles:

The lipid membrane is the most significant element of the cells in biological systems. It maintains the integrity of cells and physiology. The lipid membrane act as a barrier separating the inner cellular environment from the outer and typically serves as a boundary between the life and death of individual cells and helps in the transmission of signals across the cell boundary. A lipid bilayer is a polar membrane composed of two layers of phospholipid molecules. Membranes are sheet-like structures that form a continuous barrier around all the cells. It is almost impermeable to ions. That is why it can maintain salt concentration and pH. Lipid bilayers are made up of amphiphilic phospholipids which contain polar or hydrophilic head groups and hydrophobic tails. The tail par contains two fatty acid chains. The lipid bilayer phase also depends on the tail part and the chain length of fatty acid and the presence of unsaturation in the fatty acid chain. The lipid bilayer adopts the gel phase at lower temperatures and the fluid phase at higher temperatures via phase transition. In the presence of polar solvents like water, phospholipid molecules arrange themselves to form a lipid bilayer. Due to lipid bilayer formation, hydrophilic head parts were exposed to polar solvents while hydrophobic tail parts moved inwards. Therefore, the liposome formed from phospholipid is called the PC liposome. Lipid bilayers are prepared from lipids using the thin-film hydration method, reverse-phase evaporation, and solvent injection method [45-47].

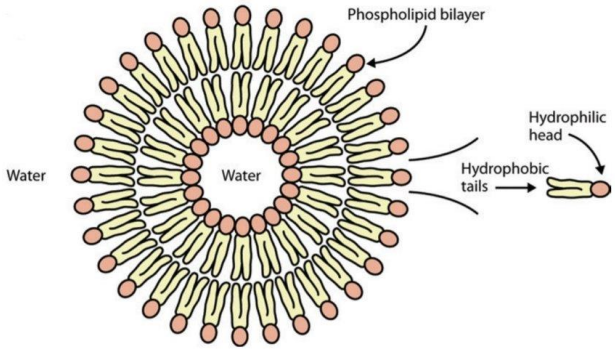

Figure 4: Structure of Lipid Vesicles.

Carbon dots has been extensively used to explore the membrane probe property unlike fluorescent organic dyes and inorganic quantum dots which exhibit cytotoxicity. The interaction of CD and lipid vesicles is mainly governed by the electrostatic force of attraction between different functional groups of CD and lipid vesicles. Lipid membrane fluidity plays an important role to alter the emission property of CD. Different lipids have different phase transition temperatures like DPPC (42 °C), DMPC (23 °C), and DOPC (-20 °C), and their fluidity plays an important role while interacting with CDs. At room temperature, DPPC is present in the sol-gel phase, DOPC is in the liquid crystalline phase, and DMPC is between the liquid crystalline and sol-gel phases. In this context, CD synthesized from DTSA and Melamine exhibit phase-dependent distinct emission of different lipid vesicles owing to their different phase transition temperatures [48]. The lipid membrane showed different interaction behavior with three isomeric carbon dots prepared from phenylenediamine (PDA) that are ortho, meta, and para-PDA carbon dots. Ortho PDA CDs are inserted into the lipid bilayer and act as a potential candidate for bio-imaging. meta-PDA CDs bring about the fusion of liposomes and para-PDA CDs also bring about aggregated forms of liposomes [49]. In order to gain the membrane dynamics of liposomes several methods have been adopted such as Förster resonance energy transfer (FRET) and bio-imaging. However, saying that the research on the interaction of liposomes and CD synthesized from different pH mediums was not explored yet. We observe Histidine Carbon Dot (HCD) obtained from different pH mediums interact completely differently with lipid vesicles. We also performed FRET between CD and NBDPE-tagged lipids to investigate the relative position of HCD. Lipids having different phase transition temperatures were also chosen to gain insight into the lipid membrane fluidity effect and stability of the HCD-liposome system.

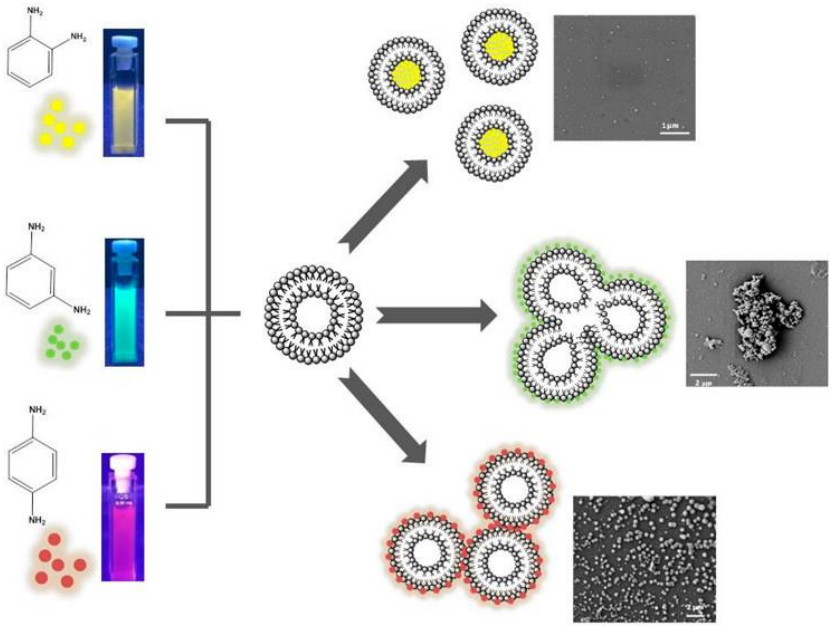

Figure 5: Carbon dots exhibit different behavior while interacting with lipid vesicles [49].

1.6 White Light Generation from CDs:

White light-emitting diodes (WLED) are the next-generation lighting device owned by their high energy efficiency, fast response, long lifetime, and high reliability [50]. In this regard, organometallic complex or organic non-metallic compounds are promising but due to their toxicity, low optical stability, and high cost restrict their application. On the other hand, CDs hold the frontier position in the WLED field thanks to their unique properties [51]. In this situation, it is quite urgent to develop a white light-emitting CD from a single precursor which is very rare. We have synthesized a one-step hydrothermal synthesis of pH-mediated Histidine CD which emits bluish-white light emission at pH <1 in water solvent and strong white light emission in ethanol solvent. However, due to resonance energy transfer (RET), the as-prepared CD is quenched in the solid state. So, we do not observe any solid-state fluorescence (SSF) but we have used a polymer matrix to explore the white light emissive property which prevents self-quenching of CD.

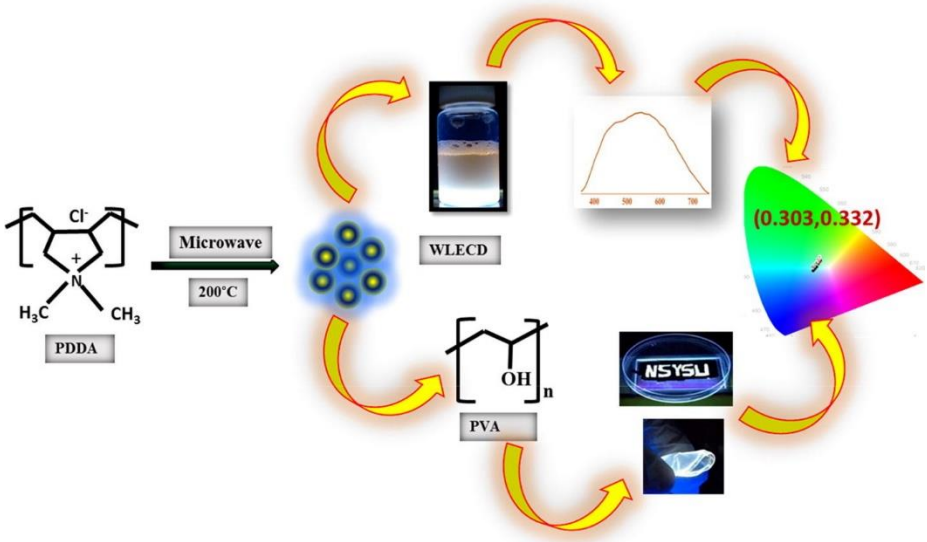

Figure 6: Generation of white light from a single precursor PDDA [52].

Experimental Section

2.1 Materials: L-Histidine was purchased from Sisco Research Laboratories Private Limited. Phospholipids DMPC(1,2-dimyristoyl-sn-glycero-3-phosphocholine), DPPC (1,2-dipalmitoyl-sn-glycero-3 phosphocholine), DOPC (1,2-dioleoyl-sn-glycero-3-phosphocholine), 14:0-12:0 NBDPC(1-Myristoyl-2-[12-[(7-nitro-2-1,3-benzoxadiazol-4-yl)amino]dodecanoyl]-snGlycero-3-Phosphocholine),14:0NBDPE(1,2-dimyristoyl-sn-glycero-3phosphoethanolamine-N-(7-nitro-2-1,3 benzoxadiazol-4-yl)(ammonium salt)were purchased from Avanti Polar Lipids. All the chemicals were used as received. We used Mili-Q water to perform all the experiments.

2.2 Synthesis of Histidine CDs:

2.2.1 Synthesis of Histidine CDs pH<1 (HCD1):

A one-step hydrothermal method was adopted to synthesize pH-mediated Histidine CDs. In a typical synthesis, 250 mg Histidine was dissolved in 10 ml Mili-Q water. The mixture was sonicated for about 30 minutes to yield a clear solution. The pH was adjusted to <1 by using 12(N) HCl. The solution was transferred to Teflon autoclaves and they were placed in a hot air oven at 200 ˚C for 12 hours to obtain CDs. It was then centrifuged at 8000 rpm for 20 minutes to remove large carbo particles followed by dialysis for 8 hours. The resulting CDs were lyophilized for about 20 hours to obtain solid HCD1. The resulting CDs were dispersed in Mili-Q water maintaining a concentration of 2mg/ml for further experiments.

2.2.2 Synthesis of Histidine CDs pH=8 (HCD8):

In a typical synthesis, 250 mg Histidine was dissolved in 10 ml Mili-Q water. The mixture was sonicated for about 30 minutes to yield a clear solution. The pH of the solution was found to be 8 and then the solution was transferred to Teflon autoclaves and they were placed in a hot air oven at 200 ˚C for 12 hours to obtain CDs. It was then centrifuged at 8000 rpm for 20 minutes to remove large carbo particles

followed by dialysis for 8 hours. The resulting CDs were lyophilized for about 20 hours to obtain solid HCD8. The resulting CDs were dispersed in Mili-Q water maintaining a concentration of 2mg/ml for further experiments.

2.3 Preparation of Carbon Dot-Liposomes Assembly:

2.3.1 Preparation of Blank Liposomes (DMPC):

The ethanol injection method was adopted to prepare blank DMPC liposomes. In a 10 ml RB, 3 ml Mili-Q water was taken and it was heated for 1 hour at 80 ˚C. After 1 hour an ethanolic solution of DMPC (1 mM) was injected into the RB. The stopper of the RB was opened for 10 minutes to evaporate the ethanol and after 10 minutes the stopper was closed and the solution was heated for another 1 hour. After that, the heating was turned off only stirring was on at 640 rpm for another 8 hours to obtain blank DMPC lipid vesicles.

2.3.2 Preparation of HCD1-DMPC Liposomes Assembly:

The ethanol injection method was adopted to prepare HCD1-DMPC Liposomes Assembly. In a 10 ml RB, 75µL HCD1 (50 µg/ml) was added followed by 2.925 ml Mili-Q. The solution was heated for 1 hour at 80 ˚C. After 1 hour an ethanolic solution of DMPC (1 mM) was injected into the RB. The stopper of the RB was opened for 10 minutes to evaporate the ethanol and after 10 minutes the stopper was closed and the solution was heated for another 1 hour. After that, the heating was turned off only stirring was on at 640 rpm for another 8 hours to obtain of HCD1-DMPC Liposomes Assembly.

2.3.3 Preparation of HCD8-DMPC Liposomes Assembly:

The ethanol injection method was adopted to prepare HCD8-DMPC Liposomes Assembly. In a 10 ml RB, 75µL HCD8 (50 µg/ml) was added followed by 2.925 ml Mili-Q. The solution was heated for 1 hour at 80 ˚C. After 1 hour an ethanolic solution of DMPC (1 mM) was injected into the RB. The stopper of the RB was opened for 10 minutes to evaporate the ethanol and after 10 minutes the stopper was closed

and the solution was heated for another 1 hour. After that, the heating was turned off only stirring was on at 640 rpm for another 8 hours to obtain of HCD8-DMPC Liposomes Assembly.

2.3.4 Preparation of HCD1-Head Tagged NBDPE DMPC Liposomes Assembly:

The ethanol injection method was adopted to prepare HCD1-Head Tagged NBDPE DMPC Liposomes Assembly. In a 10 ml RB, 75µL HCD1 (50 µg/ml) was added followed by 2.925 ml Mili-Q. The solution was heated for 1 hour at 80 ˚C. After 1 hour an ethanolic solution of DMPC (1 mM) and 35µL head-tagged NBDPE DMPC (1 mg/ml) was injected into the RB. The stopper of the RB was opened for 10 minutes to evaporate the ethanol and after 10 minutes the stopper was closed and the solution was heated for another 1 hour. After that, the heating was turned off only stirring was on at 640 rpm for another 8 hours to obtain HCD1-Head Tagged NBDPE DMPC Liposomes Assembly.

2.3.5 Preparation of HCD8-Head Tagged NBDPE DMPC Liposomes Assembly:

The ethanol injection method was adopted to prepare HCD8-Head Tagged NBDPE DMPC Liposomes Assembly. In a 10 ml RB, 75µL HCD8 (50 µg/ml) was added followed by 2.925 ml Mili-Q. The solution was heated for 1 hour at 80 ˚C. After 1 hour an ethanolic solution of DMPC (1 mM) and 35µL head-tagged NBDPE DMPC (1 mg/ml) was injected into the RB. The stopper of the RB was opened for 10 minutes to evaporate the ethanol and after 10 minutes the stopper was closed and the solution was heated for another 1 hour. After that, the heating was turned off only stirring was on at 640 rpm for another 8 hours to obtain HCD8-Head Tagged NBDPE DMPC Liposomes Assembly.

2.3.6 Preparation of HCD1-Tail Tagged NBDPE DMPC Liposomes Assembly:

The ethanol injection method was adopted to prepare HCD1-Tail Tagged NBDPE DMPC Liposomes Assembly. In a 10 ml RB, 75µL HCD1 (50 µg/ml) was added followed by 2.925 ml Mili-Q. The solution was heated for 1 hour at 80 °C. After 1 hour an ethanolic solution of DMPC (1 mM) and 35µL tail-tagged NBDPE DMPC (1 mg/ml) was injected into the RB. The stopper of the RB was opened for 10 minutes to evaporate the ethanol and after 10 minutes the stopper was closed and the solution was heated for another 1 hour. After that, the heating was turned off only stirring was on at 640 rpm for another 8 hours to obtain HCD1-Tail Tagged NBDPE DMPC Liposomes Assembly.

2.4 Instrumentation:

2.4.1 Fluorescence Spectroscopy:

FluoroMax-4p spectrofluorometer from Horiba Jobin Yvon (model: FM100) was used to record all the fluorescence spectra of HCD1 and HCD8 carbon dots and lipid-CDs assembly.

2.4.2 UV-Vis Spectrophotometer:

A Varian UV-vis spectrophotometer (Cary 100 Bio) in a quartz cuvette (10×10 mm^2) was used to record all the absorption spectra of HCD1 and HCD8 Carbon Dots.

2.4.3 Time-Correlated Single Photon Counting (TCSPC):

A Picosecond TCSPC machine from Horiba (Fluoro Cube- 01-NL) was used for lifetime measurements. Here we excited the samples at 405 nm using a picosecond diode laser and collected decays of the sample at 480 nm. A filter of 500 nm on the emission side was also placed to eliminate the scattered light. The signals were collected at a magic angle (54.75°) polarization using a photomultiplier tube (TBX-07C) as the detector. The data analysis was performed using IBH DAS

version 6 decay analysis software. We fixed the temperature at 25 °C throughout all titration experiments. The decays were fitted with a multiexponential function.

$$D(t) = \sum_{i=1}^{n} a_i \exp\left\{-\frac{t}{\tau_i}\right\}$$

where D(t) denotes normalized fluorescence decay and ai is the normalized amplitude of the decay component τ_i. The average lifetime was obtained from the equation

$$\langle\tau\rangle = \sum_{i=1}^{n} a_i \tau_i$$

The quality of fit was judged by reduced χ^2 values and corresponding residual distribution. The acceptable fit has a χ^2 near unity.

2.4.4 Confocal Laser Scanning Microscopy (CLSM):

For confocal imaging, OLYMPUS model no. IX-83 microscope was used. A multiline Argon Laser with an excitation wavelength of 405 nm was used for carbon dot-lipid assemblies. The emission was recorded by employing three different emission filters: blue region filter EM410/480, green region filter EM 490/560, and red region filter EM 565/630. A freshly prepared sample was used for this process. The slide that contained the carbon dots-liposome assembly was fixed in the right way before imaging.

Result and Discussion

3.1 Synthesis of CDs in different pH mediums and their properties:

Carbon dots synthesized from a single precursor in different pH mediums which exhibit completely different photophysical properties are found to be very rare. Herein, we have used histidine, a simple amino acid as a source of carbon. Now, one can ask instead of using other amino acids why did we choose histidine? To answer that question, we must talk about the research work performed by Yang et al in which they have synthesized pH-dependent carbon dots from serine and tryptophan [53] which exhibit completely different photophysical properties compared to each other. Furthermore, they have generated white light by fabricating CDs into polymers which prevents the self-quenching of CDs. The tuneable photophysical properties of CDs can be explained by doping of nitrogen atoms in the carbon dot core. It is to be mentioned that among serine and tryptophan, tryptophan forms the core of the carbon dot as it has an aromatic ring. The aromatic ring plays an important role to form the core of carbon dots compared to aliphatic hydrocarbons and furthermore, three nitrogen atoms defect the lattice causing multicolor emission of CDs. Similarly, histidine has an aromatic ring that can form a stable carbon dot core and it also has three nitrogen atoms that can defect the core causing multicolor emission. It is to be noted that, the pH of the medium plays an important role to synthesize carbon dots.

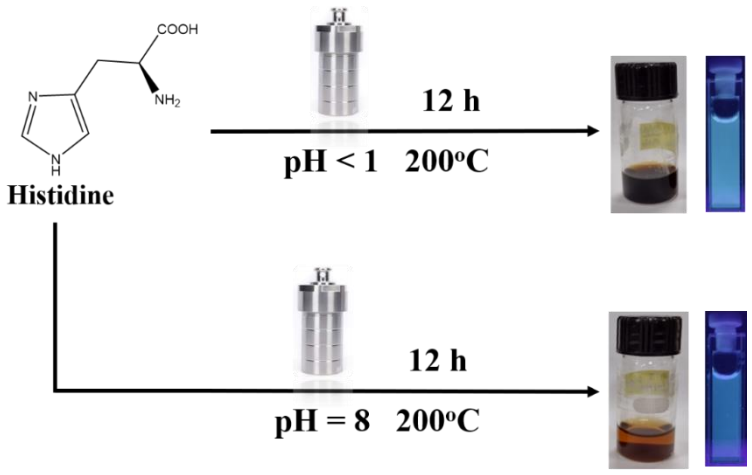

Figure 7: Reaction scheme of synthesizing pH-mediated histidine CDs.

3.2 Photophysical properties: Excitation-dependent Emission Spectroscopy:

Carbon dots synthesized from two different pH mediums pH 1 (HCD1) and pH 8 (HCD8) exhibit completely different photophysical properties compared to each other. In normal daylight, HCD1 shows dark chocolate black color whereas HCD8 shows brown color explaining the fact that acidic medium facilitated more carbonization process in case of HCD1. In highly acidic medium and hydrothermal process at high temperature and pressure leads to the dehydration of the molecule causing a large polymeric chain. While irradiating by a 365 nm UV lamp HCD1 shows bluish-white fluorescence and HCD8 shows blue fluorescence confirming the formation of different CDs in different pH mediums. In steady-state fluorescence spectroscopy, both the CD shows excitation-dependent emission. The emission spectra of HCD1 is broad ranging from 382 nm to 518 nm having a full-width half maxima (FWHM) of 136 nm upon excitation with 340 nm whereas FWHM of HCD8 is 115 (ranging from 367 nm to 452 nm) indicating the fluorescence color difference. The UV-Visible absorption reveals the absorption of HCD1 is broad compared to HCD8 justifies the broad emission spectra of HCD1. The absorption peak at 285 nm (HCD1) and 296 nm (HCD8) is due to Π-Π^* transition of C=C band whereas HCD1 has an additional absorption peak at 368 nm due to n-Π^* transition of C=O band.

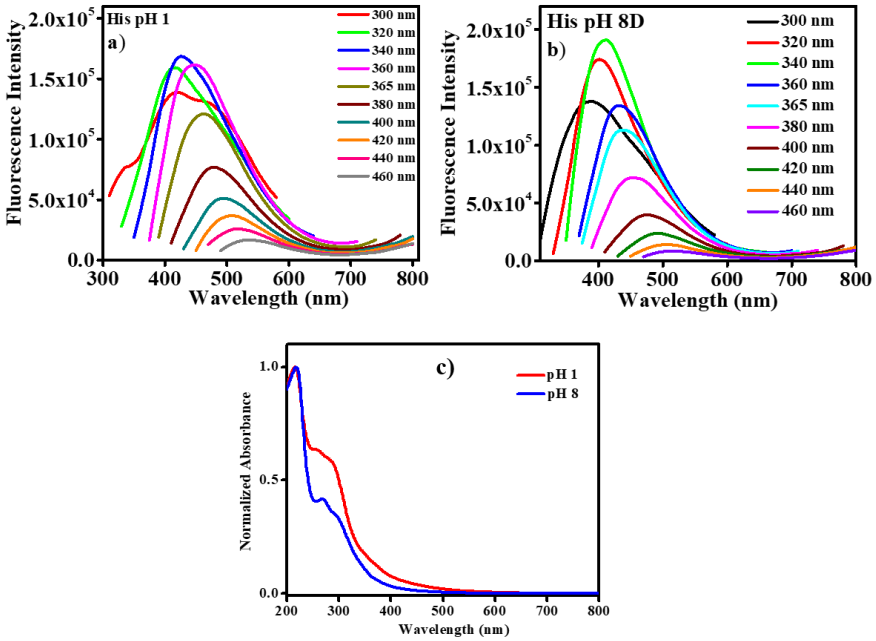

Figure 8: Excitation-dependent emission of (a) HCD1 (b) HCD8 (c) UV-Visible Spectra.

3.3 Excitation and Emission Spectra of Carbon Dots:

3.3.1 Excitation and Emission Spectra of Carbon Dots in water medium:

In excitation and emission spectra of HCD1, it was found that the maximum emission intensity peak was obtained at 428 nm, and the maximum excitation wavelength peak was obtained at 347 nm in water medium. Similarly, we also recorded the excitation and emission spectra of HCD8 in water medium, and it was found that the maximum emission intensity peak was obtained at 410 nm, and the maximum excitation wavelength peak was observed at 334 nm.

3.3.2 Excitation and Emission Spectra of Carbon Dots in ethanol medium:

In excitation and emission spectra of HCD1, it was found that the maximum emission intensity peak was obtained at 444 nm, and the

maximum excitation wavelength peak was obtained at 360 nm along with an excitation peak at 283 nm in ethanol medium. The emission of HCD1 in ethanol medium is much broader than that of water medium causing strong white light emission. Similarly, we also recorded the excitation and emission spectra of HCD8 in ethanol medium, and it was found that the maximum emission intensity peak was obtained at 400 nm, and the maximum excitation wavelength peak was observed at 334 nm.

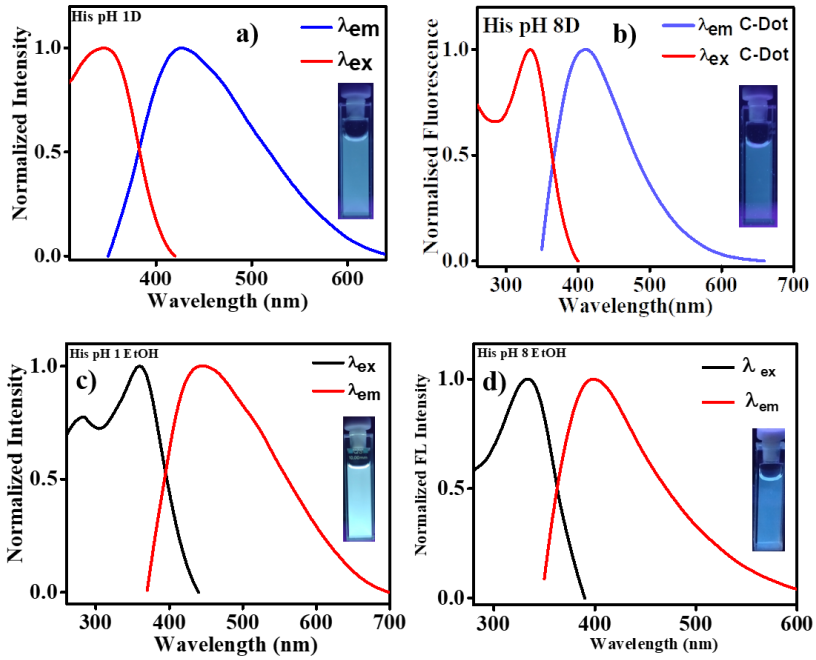

Figure 9: Excitation and Emission of HCD1 (a) in water medium (c) in ethanol medium Excitation and Emission of HCD8 (b) in water medium (d) in ethanol medium.

3.4 Solvent Dependent Study:

We also investigated the role of different solvents on the emission spectra of pH-mediated histidine carbon dots. We took a series of solvents of different polarities, namely, water, methanol, ethanol, acetonitrile, DMF, acetone, THF. We recorded their fluorescence spectra on a single irradiation wavelength of 340 nm. The solvent polarity effect was more prominent for HCD1 resulting in tuneable fluorescence emission spectra. Interestingly, HCD1 exhibits strong

white fluorescence in EtOH solvent with FWHM of 184 nm (ranging from 378 nm to 562 nm). The mechanism of this solvent-dependent emission is directly related to the synthesis of carbon dots in different pH mediums. In highly acidic medium and hydrothermal process at high temperature and pressure leads to the dehydration of the molecule causing a large polymeric chain. In TEM images it is clearly observed the presence of both aggregated and non-aggregated particles in HCD1 but on the other hand, HCD8 only contains non-aggregated particles (figure 10 a, b). EtOH is being less polar solvent than H_2O, the aggregated particles soluble more generating a fluorescence emission peak at 520 nm. The combination of both emission peaks at 428 nm and 520 nm resulting strong white fluorescence in EtOH solvent. In case of methanol solvent, the FWHM is 172 nm (ranging from 375 nm to 547 nm) and for DMF solvent, the FWHM is 164 nm (ranging from 376 nm to 540 nm). Ethanol, methanol, DMF solvents exhibit much broader emission spectra leading to white light emission for those solvents. We do not observe any significant solvent effect in case of HCD8 which confirms the presence of only non-aggregated particles. This study indicates that HCD1 contains both hydrophobic and hydrophilic parts whereas HCD8 contains only a hydrophilic part.

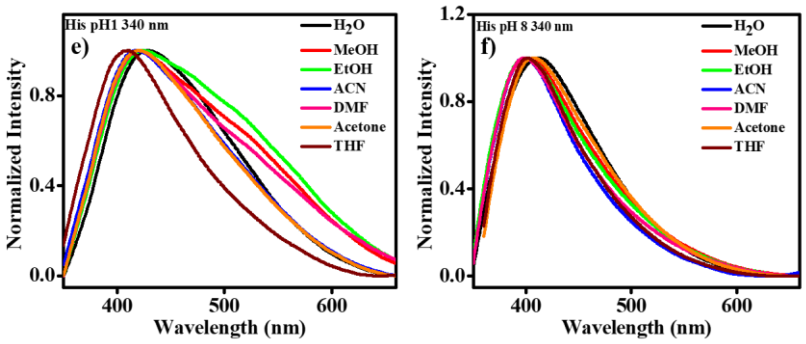

Figure 10: HR-TEM Images of HCD1 (a, b) and HCD (c, d). Solvent-dependent emission spectra of HCD1 (e) and HCD8 (f).

3.5 Concentration-Dependent Study:

As we are claiming HCD1 contains both aggregated and non-aggregated particles while on the other hand, HCD8 contains only non-aggregated particles, the concentration-dependent study is going to be very much significant in this regard. In both cases, we have adopted steady-state fluorescence spectroscopy to investigate concentration-dependent emission. We start with a very high concentration of 2 mg/ml in a 3 ml cuvette and make it half diluted in every case all the way to 0.03 mg/ml and record fluorescence emission spectra in every concentration in water solvent. In case of HCD1 concentration-dependent emission is much more prominent compared to HCD8. For HCD1 the maximum emission intensity peak was obtained at 476 nm (FWHM 171 nm) for 2 mg/ml concentration. While half diluted the solution with water the maximum emission intensity peak was observed at 452 nm (FWHM 156 nm) for 1mg/ml concentration followed by 433 nm (FWHM 145 nm) for 0.5 mg/ml and 138 nm (FWHM 138 nm) for 0.25 mg/ml concentration. So, from this observation, we can conclude that the emission peak was blue-shifted along with an increment in the intensity and shrinking of FWHM confirming the presence of aggregates. As mentioned earlier HCD1 contains both aggregated and non-aggregated particles so, while diluting the solution the aggregated particles disintegrated into non-aggregated particles resulting in a blue shift. This kind of effect was not observed in case of HCD8 which confirms the presence of only non-aggregated particles.

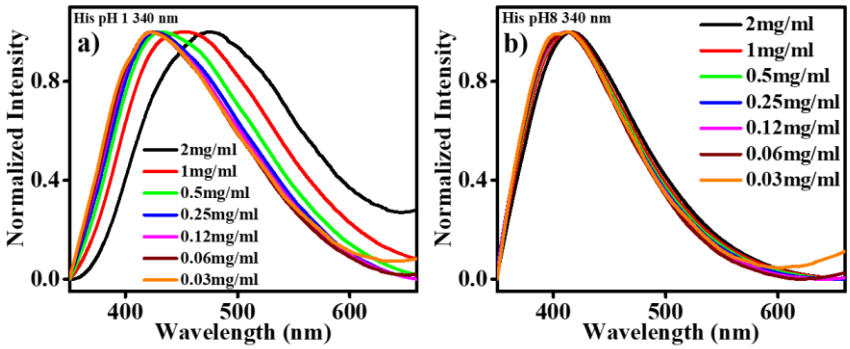

Figure 11: Concentration-dependent emission spectra of (a) HCD1 (b) HCD8.

3.6 pH-Dependent Study:

Another exciting phenomenon pH dependent study was performed by using steady-state and time-resolved fluorescence spectroscopy. The fluorescence intensity and lifetime steeply decreased in case of HCD1 while changing the pH from 6 to 7. This effect is less prominent in case of HCD8. So, HCD1 can potentially be used as a pH sensor. This phenomenon is mainly governed by the various functional groups on the surface which are accountable for the steep decrease in fluorescence intensity and lifetime of HCD1.

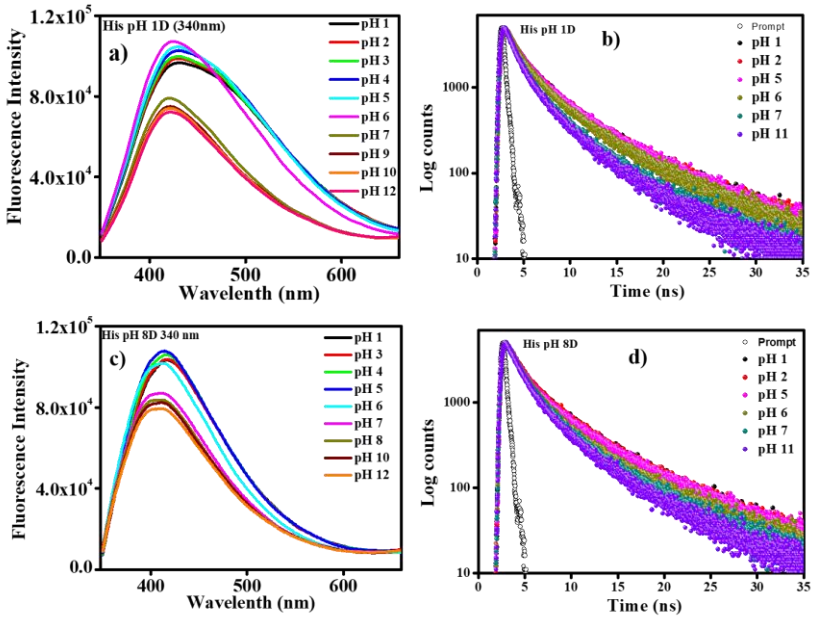

Figure 12: Steady-state and time-resolved fluorescence spectra of HCD1 (a, b) and HCD8 (c, d) respectively.

3.7 Interaction of Carbon Dots-Liposome System:

To gain a photophysical insight into the interaction between HCD and DMPC liposome the emission property of HCD was exploited through steady-state and time-resolved fluorescence spectroscopy. HCD1 showed a significant blue shift of 7 nm (from 457 nm to 450 nm) whereas HCD8 barely showed any shift. This study indicates that HCD1 experiences a distinctly less polar chemical environment while interacting with DMPC liposome. The fluorescence lifetime decreased from 2.89 ns to 2.66 ns indicating a more confined environment. This trend was not observed in case of HCD8 signifies the discriminatory behavior of lipid vesicles towards HCD.

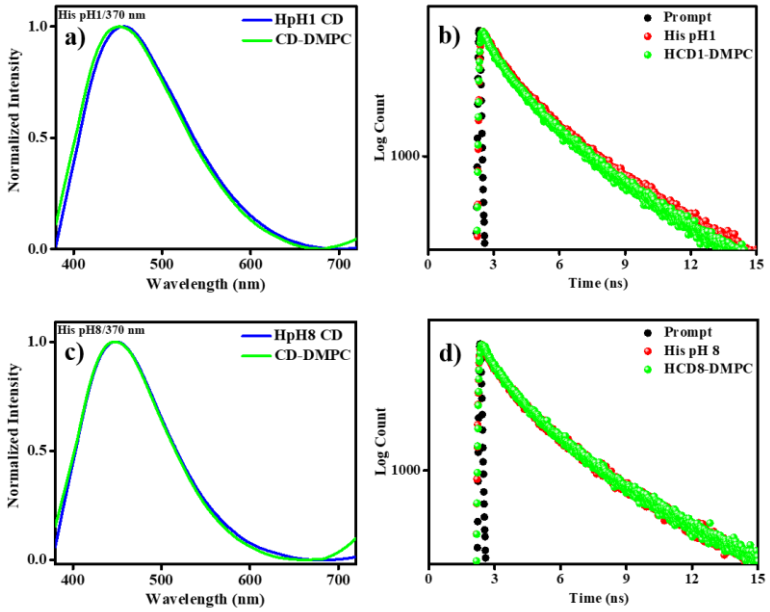

Figure 13: Steady-state and time-resolved fluorescence spectra of HCD1-DMPC liposome system (a, b) and HCD8-DMPC liposome system (c, d) respectively.

To support the spectroscopic data, imaging techniques such as CLSM and SEM were adopted. In CLSM (figure 14) the fluorescence signal coming from the bilayer region in case of HCD1 indicates that HCD1 is located in the bilayer region of DMPC lipid vesicles. However, while interacting with HCD8 the lipid vesicles undergo aggregation resulting increase in size of lipid vesicles. We did not observe any

fluorescence signal in case of HCD8-DMPC system. The morphological changes in lipid vesicles upon interacting with HCD were studied by SEM images (figure 15). SEM images reveal that lipid vesicles hold their morphology upon interacting with HCD1 but undergo aggregation while interacting with HCD8 which supports the CLSM data.

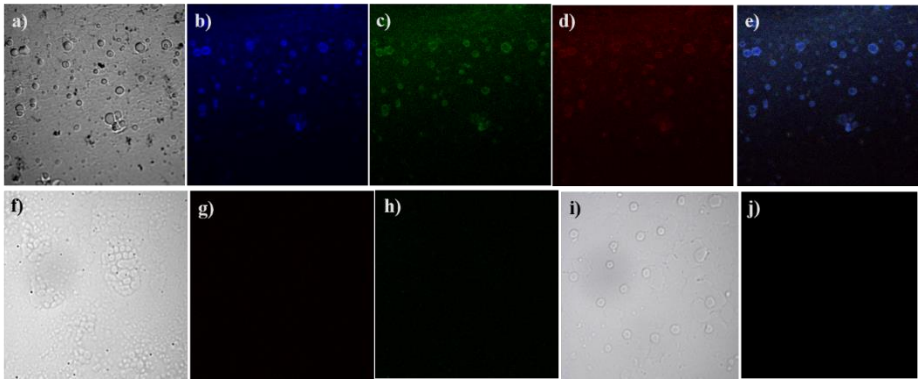

Figure 14: CLSM Images of DMPC liposome and His CD pH = 1 in (a) Bright Field (b) Blue (c) Green (d) Red (e) Merged. CLSM Images of DMPC liposome and His CD pH = 8 in (f) Bright Field (g) Blue (h) Green (i) Blank DMPC Liposome (j) Blue region.

The discriminatory behavior of lipid vesicles toward HCD can possibly be explained by the hydrophobicity of HCD and the electrostatic force of attraction of different functional groups in HCD-DMPC system. As mentioned earlier HCD1 contains both hydrophobic and hydrophilic parts that help to penetrate into lipid vesicles and locate in the bilayer region. On the other hand, HCD8 is being extremely hydrophilic, the electrostatic force of attraction of different functional groups in HCD8-DMPC system results in cross-linking with more than one lipid vesicle causing aggregation. After causing aggregation of lipid vesicles, HCD8 aggregates themselves resulting in fluorescence turn-off in CLSM measurement due to the self-quenching phenomenon of CD in solid-state. However, we do get confocal fluorescence signal for HCD1-DMPC system as HCD1 is located in the bilayer region preventing self-quenching. To gain an insight into the possible location of HCD in

HCD-DMPC system we performed FRET between NBDPE-tagged lipid vesicles and HCD. This combination was chosen due to the large spectral overlap where HCD acts as a donor and NBDPE acts as an acceptor (figure 16).

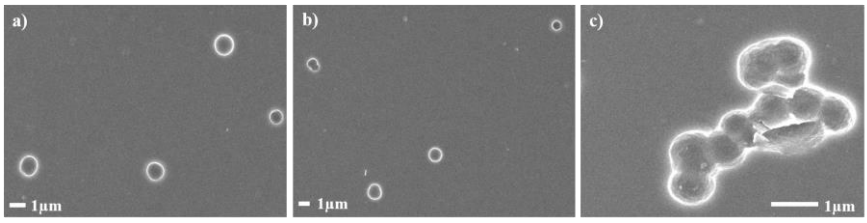

Figure 15: SEM Images of (a) Blank DMPC liposome (b) His pH1-DMPC liposome and (c) His pH8-DMPC liposome.

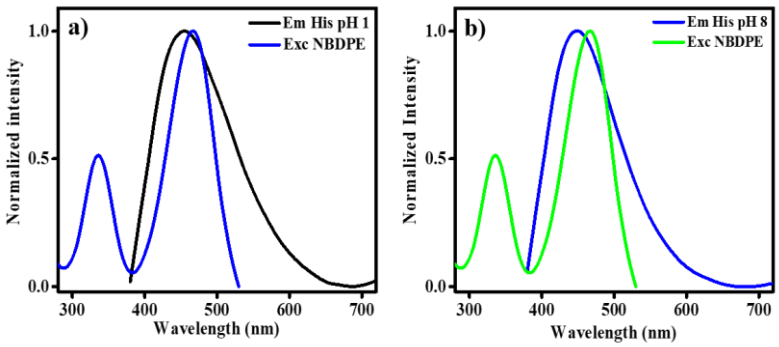

Figure 16: Spectral Overlap between (a) His pH 1 – NBDPE and (b) His pH 8 – NBDPE.

To investigate the possible position of HCD we have used both head and tail-tagged NBDPE-DMPC lipids. The decrease in emission intensity of HCD1 along with a concurrent increase in emission intensity of NBDPE suggests energy transfer phenomenon. The energy transfer efficiency of tail-tagged NBDPE-HCD1 is calculated 11% from time-resolved and 17% from steady-state fluorescence measurement. Similarly, in case of head-tagged NBDPE-HCD1, the energy transfer efficiency is 15% from time-resolved and 21% from steady-state fluorescence spectroscopy. This result signifies HCD1 may be located somewhere between the membrane bilayer and interfacial region. In case of HCD1-liposome system, both static and

dynamic quenching happening which can be proved via steady-state and time-resolved fluorescence spectroscopy while on the other hand in HCD8-liposome system, only static quenching is happening. In case of HCD1-head tagged DMPC liposome the energy transfer efficiency is higher than that of HCD1-tail tagged DMPC liposome. The FRET equation is:

$$E = \frac{1}{1 + (R / R_0)^6} = 1 - \frac{I}{I_0} = 1 - \frac{F}{F_0}$$

Here E is energy efficiency, R is the distance between donor and acceptor, R_0 is the Forster distance, F is the fluorescence intensity in presence of quencher, F_0 is the fluorescence intensity in absence of quencher, I is the lifetime of fluorophore in presence of quencher and I_0 is the lifetime of fluorophore in absence of quencher.

This result matched our confocal images where HCD1 slightly penetrates into the liposome and closer to the interfacial region compare to the bilayer region. On the other hand, HCD8 caused aggregation of DMPC liposomes so in the time-resolved fluorescence data there is no change in lifetime was observed while in the steady-state measurement the quenching is 11% indicating only static quenching with the head tagged NBDPE dye and HCD8 carbon dot.

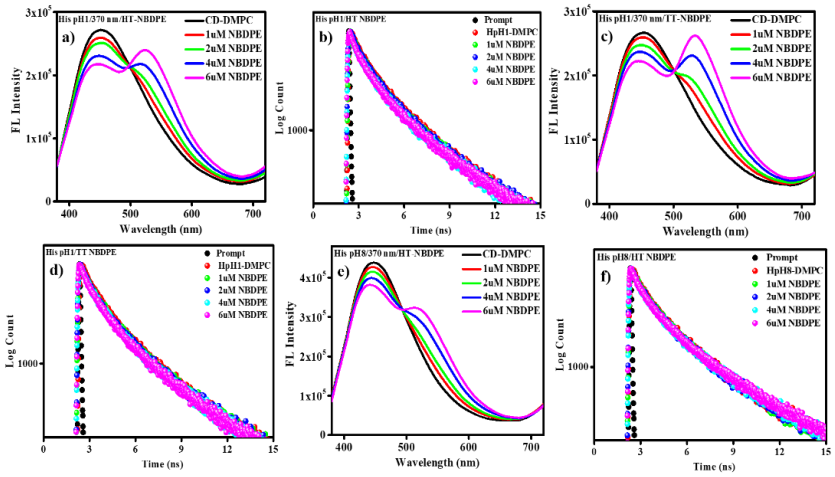

Figure 17: Energy Transfer of His pH 1-NBDPE (Head-Tagged) (a) Steady-State (b) Time-Resolved Fluorescence Spectroscopy. Energy Transfer of His pH 1-NBDPE (Tail-Tagged) (c) Steady-State (d) Time-Resolved Fluorescence Spectroscopy. Energy Transfer of His pH 8-NBDPE (Head-Tagged) (e) Steady-State (f) Time-Resolved Fluorescence Spectroscopy.

3.8 Generation of White-Light: Carbon Dot-Polymer Composite:

HCD1 exhibits bluish-white emission in water medium and strong white light emission in ethanol medium. However, saying that in the solid state, HCD1 do not show any fluorescence due to self-quenching of carbon dot which restricts their application in white light generation in solid state. But carbon dot-polymer system can solve the problem as polymer resists carbon dots from self-quenching which brings us to the generation of white light in solid state. Here we used polyethyleneimine (PEI) as a polymer to prevent the self-quenching of HCD1 which allows us to generate white light emission in the solid state. We have also recorded the fluorescence emission spectra of HCD-PEI system. In steady-state fluorescence measurement, excitation-independent emission was observed and maximum emission intensity peak was observed at 573 nm. The FWHM of the HCD1-PEI system covers the whole visible spectrum ranging from 474 nm to 679 nm (FWHM 204 nm) which is accountable for the strong white light emission (figure 18). The maximum excitation wavelength peak was

obtained at 366 nm along with an excitation peak at 437 nm. The excitation spectrum is extremely broad accountable for the broadness of the emission spectra of the HCD1-PEI system.

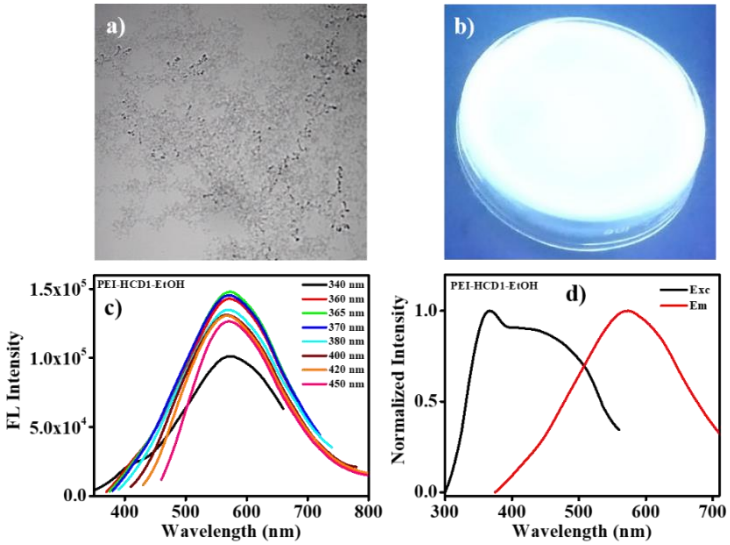

Figure 18: Confocal image of HCD1(a), picture of HCD1-PEI system under 365 nm UV lamp (b), excitation-independent emission spectra of HCD1-PEI system (c), Excitation and emission spectra of HCD1-PEI system (d).

Conclusion

In summary, we have synthesized pH-mediated Histidine carbon dots which exhibit completely different photophysical properties compared to each other. From the above studies, we summarized the following important observations:

(1) The pH of the medium play an important role in the preparation of different emissive carbon dots.

(2) His-pH1 CD showed bluish-white emission behavior in water but was strongly white emissive in ethanol due to the aggregation of the CDs in ethanol. But the His-pH8 CD showed blue emission in both ethanol and water medium.

(3) His-pH1 CD emission drastically changed (decreased) as soon as the pH of the solution was decreased from pH 6 to pH 7. So, it can act as pH-based sensor.

(4) The concentration-dependent emission spectra of His-pH1 CD showed that the emission peak was blue-shifted along with the increment in the intensity which suggests the presence of the aggregates.

(5) Lipid membranes (DMPC) exhibit discriminatory behavior toward CDs synthesized from different pH mediums. His pH1 CD is located in the bilayer region whereas, His pH8 caused aggregation of lipid vesicles.

(6) White light emission was obtained by embedding His pH1 CD into PEI polymer matrix which resist quenching of CD, unlike in the solid state.

References

[1] Santamaria, A. Historical overview of nanotechnology and nanotoxicology. *Nanotoxicity: methods and protocols* **2012**, 1-12.

[2] Feynman, R. There's plenty of room at the bottom. *In Feynman and computation* **2012**, 63-76.

[3] Bayda, S.; Adeel, M.; Tuccinardi, T.; Cordani, M.; Rizzolio, F. The history of nanoscience and nanotechnology: from chemical–physical applications to nanomedicine. *Molecules* **2019**, *25*, 112.

[4] Zhang, L.; Webster, T. J. Nanotechnology and nanomaterials: promise for improved tissue regeneration. *Nano today* **2009**, *4*, 66-80.

[5] Singh, M.; Singh, S.; Prasad, S.; Gambhir, I. S. Nanotechnology in medicine and antibacterial effect of silver nanoparticles. *Dig. J. Nanomater. Biostructures* **2008**, *3*, 115-122.

[6] Ngoy, J. M.; Wagner, N.; Riboldi, L.; Bolland, O. A CO2 capture technology using multi-walled carbon nanotubes with polyaspartamide surfactant. *Energy Procedia* **2014**, *63*, 2230-2248.

[7] Sardar, R.; Funston, A. M.; Mulvaney, P.; Murray, R. W. Gold nanoparticles: past, present, and future. *Langmuir* **2009**, *25*, 13840-13851.

[8] Sperling, R. A.; Gil, P. R.; Zhang, F.; Zanella, M.; Parak, W. J. Biological applications of gold nanoparticles. *Chem. Soc. Rev.* **2008,** *37*, 1896-1908.

[9] Yu, S. J.; Yin, Y. G.; Liu, J. F. Silver nanoparticles in the environment. *Environ. Sci.: Process. Impacts* **2013**, *15*, 78-92.

[10] Sun, W. T.; Yu, Y.; Pan, H. Y.; Gao, X. F.; Chen, Q.; Peng, L. M. CdS quantum dots sensitized TiO2 nanotube-array photoelectrodes. *J. Am. Chem. Soc.* **2008**, *130*, 1124-1125.

[11] Danek, M.; Jensen, K. F.; Murray, C. B.; Bawendi, M. G. Synthesis of luminescent thin-film CdSe/ZnSe quantum dot

composites using CdSe quantum dots passivated with an overlayer of ZnSe. *Chem. Mater.* **1996**, *8*, 173-180.

[12] Mansha, M.; Khan, I.; Ullah, N.; Qurashi, A. Synthesis, characterization and visible-light-driven photoelectrochemical hydrogen evolution reaction of carbazole-containing conjugated polymers. *Int. J. Hydrog. Energy* **2017**, *42*, 10952-10961.

[13] Kralj, S.; Makovec, D. Magnetic assembly of superparamagnetic iron oxide nanoparticle clusters into nanochains and nanobundles. *ACS Nano* **2015**, *9*, 9700-9707.

[14] Dreaden, E. C.; Alkilany, A. M.; Huang, X.; Murphy, C. J.; El-Sayed, M. A. The golden age: gold nanoparticles for biomedicine. *Chem. Soc. Rev.* **2012**, *41*, 2740-2779.

[15] Agam, M. A.; Guo, Q. Electron beam modification of polymer nanospheres. *J. Nanosci. Nanotechnol.* **2007**, *7*, 3615-3619.

[16] Sun, Y.; Xia, Y. Shape-controlled synthesis of gold and silver nanoparticles. *Science* **2002**, *298*, 2176-2179.

[17] Zhang, Z.; Bando, K.; Mochizuki, K.; Taguchi, A.; Fujita, K.; Kawata, S. Quantitative evaluation of surface-enhanced Raman scattering nanoparticles for intracellular pH sensing at a single particle level. *Anal. Chem.* **2019**, *91*, 3254-3262.

[18] Ding, H.; Yu, S. B.; Wei, J. S.; Xiong, H. M. Full-color light-emitting carbon dots with a surface-state-controlled luminescence mechanism. *ACS Nano* **2016**, *10*, 484-491.

[19] Lim, S. Y.; Shen, W.; Gao, Z. Carbon quantum dots and their applications. *Chem. Soc. Rev.* **2015**, *44*, 362-381.

[20] Georgakilas, V.; Perman, J. A.; Tucek, J.; Zboril, R. Broad family of carbon nanoallotropes: classification, chemistry, and applications of fullerenes, carbon dots, nanotubes, graphene, nanodiamonds, and combined superstructures. *Chem. Rev.* **2015**, *115*, 4744-4822.

[21] LeCroy, G. E.; Sonkar, S. K.; Yang, F.; Veca, L. M.; Wang, P.; Tackett, K. N.; Sun, Y. P. Toward structurally defined carbon dots as ultracompact fluorescent probes. *ACS Nano* **2014**, *8*, 4522-4529.

[22] Emam, A. N.; Loutfy, S. A.; Mostafa, A. A.; Awad, H.; Mohamed, M. B. Cyto-toxicity, biocompatibility and cellular response of carbon dots–plasmonic based nano-hybrids for bioimaging. *RSC Adv.* **2017**, *7*, 23502-23514.

[23] Ju, B.; Wang, Y.; Zhang, Y. M.; Zhang, T.; Liu, Z.; Li, M.; Xiao-An Zhang, S. Photostable and low-toxic yellow-green carbon dots for highly selective detection of explosive 2, 4, 6-trinitrophenol based on the dual electron transfer mechanism. *ACS Appl. Mater. Interfaces* **2018**, *10*, 13040-13047.

[24] Liu, Y.; Zhou, L.; Li, Y.; Deng, R.; Zhang, H. Highly fluorescent nitrogen-doped carbon dots with excellent thermal and photo stability applied as invisible ink for loading important information and anti-counterfeiting. *Nanoscale* **2017**, *9*, 491-496.

[25] Jin, J.; Chen, C.; Li, H.; Cheng, Y.; Xu, L.; Dong, B.; Dai, Q. Enhanced performance and photostability of perovskite solar cells by introduction of fluorescent carbon dots. *ACS Appl. Mater. Interfaces* **2017**, *9*, 14518-14524.

[26] Hill, S. A.; Benito-Alifonso, D.; Morgan, D. J.; Davis, S. A.; Berry, M.; Galan, M. C. Three-minute synthesis of sp 3 nanocrystalline carbon dots as non-toxic fluorescent platforms for intracellular delivery. *Nanoscale* **2016**, *8*, 18630-18634.

[27] Xu, X.; Ray, R.; Gu, Y.; Ploehn, H. J.; Gearheart, L.; Raker, K.; Scrivens, W. A. Electrophoretic analysis and purification of fluorescent single-walled carbon nanotube fragments. *J. Am. Chem. Soc.* **2004**, *126*, 12736-12737.

[28] Demchenko, A. P.; Dekaliuk, M. O. Novel fluorescent carbonic nanomaterials for sensing and imaging. *Methods Appl. Fluoresc.* **2013**, *1*, 042001.

[29] Guo, X.; Wang, C. F.; Yu, Z. Y.; Chen, L.; Chen, S. Facile access to versatile fluorescent carbon dots toward light-emitting diodes. *Chem. Commun.* **2012**, *48*, 2692-2694.

[30] Li, H.; He, X.; Kang, Z.; Huang, H.; Liu, Y.; Liu, J.; Lee, S. T. Water-soluble fluorescent carbon quantum dots and photocatalyst design. *Angew. Chem. Int. Ed.* **2010**, *49*, 4430-4434.

[31] Singh, V., Mishra, A. K. White light emission from a mixture of pomegranate extract and carbon nanoparticles obtained from the extract. *J. Mater. Chem. C* **2016**, *4*, 3131-3137.

[32] Shi, W.; Guo, F.; Han, M.; Yuan, S.; Guan, W.; Li, H.; Kang, Z. N, S co-doped carbon dots as a stable bio-imaging probe for detection of intracellular temperature and tetracycline. *J. Mater. Chem. B* **2017**, *5*, 3293-3299.

[33] Dhanush, C.; Aravind, M. K.; Ashokkumar, B.; Sethuraman, M. G. Synthesis of blue emissive fluorescent nitrogen doped carbon dots from Annona squamosa fruit extract and their diverse applications in the field of catalysis and bio-imaging. *J. Photochem. Photobiol. A: Chem.* **2022**, *432*, 114097.

[34] Yue, L.; Li, H.; Sun, Q.; Zhang, J.; Luo, X.; Wu, F.; Zhu, X. Red-emissive ruthenium-containing carbon dots for bioimaging and photodynamic cancer therapy. *ACS Appl. Nano Mater.* **2020**, *3*, 869-876.

[35] Das, G. S.; Shim, J. P.; Bhatnagar, A.; Tripathi, K. M.; Kim, T. Biomass-derived carbon quantum dots for visible-light-induced photocatalysis and label-free detection of Fe (III) and ascorbic acid. *Sci. Rep.* **2019**, *9*, 1-9.

[36] Tyagi, A.; Tripathi, K. M.; Singh, N.; Choudhary, S.; Gupta, R. K. Green synthesis of carbon quantum dots from lemon peel waste: applications in sensing and photocatalysis. *RSC Adv.* **2016**, *6*, 72423-72432.

[37] Li, M.; Chen, T.; Gooding, J. J.; Liu, J. Review of carbon and graphene quantum dots for sensing. *ACS Sens.* **2019**, *4*, 1732-1748.

[38] Cailotto, S.; Negrato, M.; Daniele, S.; Luque, R.; Selva, M.; Amadio, E.; Perosa, A. Carbon dots as photocatalysts for organic synthesis: metal-free methylene–oxygen-bond photocleavage. *Green Chem.* **2020**, *22*, 1145-1149.

[39] Pokropivny, V.V.; Skorokhod, V.V. Classification of nanostructures by dimensionality and concept of surface forms engineering in nanomaterial science. *Mater. Sci. Eng. C* **2007**, *27*, 990–993.

[40] Jeevanandam, J.; Barhoum, A.; Chan, Y. S.; Dufresne, A.; Danquah, M. K. Review on nanoparticles and nanostructured materials: history, sources, toxicity, and regulations. *Beilstein J. Nanotechnol*. **2018**, *9*, 1050–1074.

[41] Anwar, S.; Ding, H.; Xu, M.; Hu, X.; Li, Z.; Wang, J.; Bi, H. Recent advances in synthesis, optical properties, and biomedical applications of carbon dots. *ACS Appl. Bio Mater.* **2019**, *2*, 2317-2338.

[42] Kumar, P.; Dua, S.; Kaur, R.; Kumar, M.; Bhatt, G. A review on advancements in carbon quantum dots and their application in photovoltaics. *RSC Adv.* **2022**, *12*, 4714-4759.

[43] Li, H.; Kang, Z.; Liu, Y.; Lee, S. T. Carbon nanodots: synthesis, properties and applications. *J. Mater. Chem.* **2012**, *22*, 24230-24253.

[44] Zhu, S.; Song, Y.; Zhao, X.; Shao, J.; Zhang, J.; Yang, B. The photoluminescence mechanism in carbon dots (graphene quantum dots, carbon nanodots, and polymer dots): current state and future perspective. *Nano Res.* **2015**, *8*, 355-381.

[45] Kanwa, N.; De, S. K.; Adhikari, C.; Chakraborty, A. Spectroscopic study of the interaction of carboxyl-modified gold nanoparticles with liposomes of different chain lengths and controlled

drug release by layer-by-layer technology. *J. Phys. Chem. B* **2017**, *121*, 11333-11343.

[46] Bangham, A. D.; De Gier, J.; Greville, G. D. Osmotic properties and water permeability of phospholipid liquid crystals. *Chem. Phys. Lipids* **1967**, *1*, 225-246.

[47] Szoka Jr, F.; Papahadjopoulos, D. Procedure for preparation of liposomes with large internal aqueous space and high capture by reverse-phase evaporation. *Proc. Natl. Acad. Sci.* **1978**, *75*, 4194-4198.

[48] De, S. K.; Maity, A.; Bagchi, D.; Chakraborty, A. Lipid phase dependent distinct emission behaviour of hydrophobic carbon dots: C-dot based membrane probes. *Chem. Commun.* **2021**, *57*, 9080-9083.

[49] Kanwa, N.; Chakraborty, A. Discriminatory Interaction Behavior of Lipid Vesicles toward Diversely Emissive Carbon Dots Synthesized from Ortho, Meta, and Para Isomeric Carbon Precursors. *Langmuir* **2020**, *36*, 10628-10637.

[50] de Ranieri, E.; Moscatelli, A.; Pulizzi, F.; Vaughan, O. Our choice from the recent literature. *Nat. Nanotechnol.* **2015**, *10*, 732.

[51] Xu, J.; Miao, Y.; Zheng, J.; Wang, H.; Yang, Y.; Liu, X. Carbon dot-based white and yellow electroluminescent light emitting diodes with a record-breaking brightness. *Nanoscale* **2018**, *10*, 11211-11221.

[52] Madhu, M.; Chen, T. H.; Tseng, W. L. White-light emission of single carbon dots prepared by hydrothermal carbonization of poly (diallyldimethylammonium chloride): Applications to fabrication of white-light-emitting films. *J. Colloid Interface Sci.* **2019**, *556*, 120-127.

[53] Lu, S.; Cong, R.; Zhu, S.; Zhao, X.; Liu, J.; S. Tse, J.; Yang, B. pH-dependent synthesis of novel structure-controllable polymer-carbon nanodots with high acidophilic luminescence and super carbon dots assembly for white light-emitting diodes. *ACS Appl. Mater. Interfaces* **2016**, *8*, 4062-4068.